
PERGAMON

Journal of Quantitative Spectroscopy & Radiative Transfer 82 (2003) 517–531

Journal of Quantitative Spectroscopy & Radiative Transfer

www.elsevier.com/locate/jqsrt

A simple analytical parameterization for the water vapor millimeter wave foreign continuum

Q. Ma[a,*], R.H. Tipping[b]

[a] *Department of Applied Physics, Columbia University, NASA/Goddard Institute for Space Studies, 2880 Broadway, New York, NY 10025, USA*

[b] *Department of Physics and Astronomy, University of Alabama, Tuscaloosa, AL 35487, USA*

Received 23 December 2002; received in revised form 28 February 2003; accepted 3 March 2003

Abstract

We present a theoretical calculation of the millimeter wave foreign continuum due to colliding pairs of H_2O–N_2 molecules. The theory is formulated using the symmetrized spectral density which ensures that the principle of detailed balance is satisfied. It is based on the Lanczos algorithm, and the resulting tri-diagonal matrix is written in terms of continued fractions. The calculations are carried out in the coordinate representation in which the basis functions are delta functions whose arguments are the angular variables necessary to specify the molecular orientations. In this representation, the anisotropic interaction potential responsible for the continuum absorption is diagonal, and the ensemble averages over the states become multidimensional integrations. These are computed using the Monte Carlo method. The results, computed for a range of temperatures relevant to the atmosphere, are compared to laboratory measurements and to widely used empirical models. For easy use, we fit our results for the absorption coefficient to a simple analytic function of frequency and temperature.

Keywords: Millimeter wave absorption; Water vapor; Lanczos algorithm

1. Introduction

Accurate specification of continuum absorption is essential to the accuracy of satellite retrievals. This applies to microwave sounding instruments such as NAST-M, but is particularly true for the Microwave Limb Sounder (MLS) [1] where the minimum retrievable altitude for tropospheric water vapor will be determined from the baseline (what is left after the line contribution is removed). Since the baseline is the atmospheric continuum, which depends on moisture, temperature, and pressure, accurate constituent retrievals depend critically on getting the background absorption correct.

* Corresponding author.
E-mail address: qma@giss.nasa.gov (Q. Ma).

0022-4073/03/$ - see front matter
doi:10.1016/S0022-4073(03)00175-4

At present, our understanding of the problem is not satisfactory. There are only a few laboratory measurements of the water vapor millimeter continuum absorption that have been carried out [2]. The most recent ones are by Liebe's group at 138 GHz [3,4] and by Bauer's group at 190, 213, 153, 239 and 350 GHz [5–9]. Due to experimental difficulties, these results contain large uncertainties. The situation is even worse for the foreign continuum because, in general, these values are small and they have to be derived by subtracting the self-continuum and local line contributions from the raw data. In addition, except for Liebe's data at 138 GHz which contain values obtained at $T = 282$ K, all others for 153, 190, 213, 239, and 350 GHz provided by Bauer's group are obtained at room temperature and above. At present the temperature dependence of the continuum absorption is not well known, so that extrapolation of these values to much lower temperatures is very risky, and there is no proper way to estimate how much error could be introduced.

On the other hand, of the several empirical models available [10–12], none of them meets the desired accuracy, or works satisfactorily for all atmospheric conditions. This is not surprising since all empirical models assumed to be applicable for a wide range of temperature are constructed mainly by matching laboratory data, which are available only for a limited high temperature part. More specifically, the most widely used Liebe MPM89 model [10] is based on their measurements at 138 GHz, and the new version, MPM93 [11], is a combination of their own data and others, including Bauer's data for 190 and 213 GHz. It turns out that the MPM93 model differs significantly from the MPM89 version both for the self- and foreign continuum, and neither of them is able to predict the continuum well. By analyzing differences between these two models, Rosenkranz concluded that the best model is a combination of the MPM93 self-continuum model plus the MPM89 foreign continuum. This latter combination, labeled by some people as ROS98, is currently the favored model. Recently, measurements of the submillimeter atmospheric transmission made on Mauna Kea during extremely dry El Niño conditions by Pardo et al. [13] suggest that the H_2O continuum-like terms defined in MPM93 and MPM89 are not accurate in the submillimeter range, and they found that their best-fit values lie between those predicted by these two models. Given the fact that in these extremely dry air conditions the foreign continuum is dominant and is identical in both ROS98 and MPM89, their conclusion is also applicable to ROS98. We note that the temperature dependence of the foreign continuum in the MPM89 model (and also in ROS98) has been simply assumed to be T^{-3}. This assumption implies that the spectral density $F(\omega)$, which contains all dynamical information about the broadening process, does not depend on temperature, and this is not consistent with our physical understanding of the collisional process. In summary, there is a definite need to refine the empirical models.

Theoretical calculations have made a major contribution to our understanding of the water vapor continuum. However, there is a lack of theoretical work from which one is able to predict the millimeter wave foreign continuum quantitatively accurately. Although the recent far-wing line shape theory works well in calculating continuum absorptions for the infrared spectral region [14–16] its applicability in the millimeter wave region is questionable. The main reason for this is not the far-wing line shape theory itself, but the band average approximation, the usual procedure introduced to simplify calculations. This approximation is not valid for the millimeter wave spectral range. Fortunately, an alternative theoretical method is available to calculate millimeter wave continua. This is the Lanczos algorithm which has been used successfully to calculate the millimeter wave self-continuum [17]. With the Lanczos algorithm, we have shown that the spectral density can be written as a continued fraction, and by using the lowest-order truncation, we can calculate the

absorption. However, for calculating the foreign continuum due to H_2O–N_2 collision pairs, there is no contribution to the absorption from the lowest-order truncation of the continued fractions and, thus, one has to consider higher-order fractions that are intractable using standard computational methods.

A breakthrough to address this problem arose indirectly from our far-wing line shape research. In the past few years, we have developed a first-principles far-wing line shape formalism and applied it to H_2O continuum absorption in the infrared spectral region [14–16]. To overcome convergence problems, we introduced the coordinate representation in which the eigenfunctions of the orientations of the two interacting molecules are chosen as the complete set of basis functions in Hilbert space. In this representation, the interaction potential is diagonal, ensemble averages become multidimensional integrations over the continuous angular variables, and as many states as desired can be included in the calculations. The convergence criterion is thus transformed to the feasibility of calculating these multidimensional integrations, and these can be successfully evaluated using the Monte Carlo method. Recently, by using the coordinate representation and the Monte Carlo method, we have carried out preliminary calculations for the millimeter wave foreign continuum based on the Lanczos algorithm and we obtained results in reasonable agreement with both experimental data and empirical models [18]. In the present paper, we present an improved formulation starting from the symmetrized spectral density instead of the standard, non-symmetrized one used previously. This has two major advantages: first, because of symmetry the numerical calculations are reduced by a factor of 2; and second, detailed balance can be maintained at every order of truncation of the continued fractions. As a result, we feel that the results are more accurate than those obtained without the symmetrization.

2. General formalism

2.1. Absorption coefficient and spectral density

As is well known, the absorption of radiation at frequency ω per unit volume of a gaseous sample in thermal equilibrium at temperature T is characterized by the absorption coefficient $\alpha(\omega)$:

$$\alpha(\omega) = \frac{4\pi^2}{3\hbar c}\omega(e^{\beta\hbar\omega} - 1)F(\omega)$$

$$= \frac{4\pi^2}{3\hbar c}\omega \tanh(\beta\hbar\omega/2)\{F(\omega) + F(-\omega)\}, \tag{1}$$

where the spectral density $F(\omega)$ is the Fourier transform of the correlation function $C(t)$ of the dipole moment operator; that is

$$F(\omega) = \frac{1}{\pi}\,\mathrm{Re}\int_0^\infty e^{i\omega t}C(t)\,dt \tag{2}$$

and

$$C(t) = Tr(\vec{\mu}^\dagger e^{-iHt}\rho\vec{\mu}e^{iHt}), \tag{3}$$

where $\vec{\mu}$ is the dipole moment operator of the sample and ρ is the density matrix. For later convenience, we introduce the symmetric correlation function $\tilde{C}(t) \equiv C(t + i\beta\hbar/2)$ and its Fourier

transform, the symmetric spectral density $\tilde{F}(\omega)$. In terms of the later, one can express $\alpha(\omega)$ as

$$\alpha(\omega) = \frac{8\pi^2}{3\hbar c}\,\omega \sinh(\beta\hbar\omega/2)\tilde{F}(\omega). \tag{4}$$

It is easy to show that $\tilde{C}(-t) = \tilde{C}(t)$, $\tilde{F}(-\omega) = \tilde{F}(\omega)$, and, in addition, $\tilde{F}(\omega) = \exp(\beta\hbar\omega/2)F(\omega)$. With the expressions for $\tilde{C}(\mathrm{t})$,

$$\begin{aligned}\tilde{C}(t) &= Tr(\sqrt{\rho}\vec{\mu}^{\dagger}\mathrm{e}^{-\mathrm{i}Ht}\sqrt{\rho}\vec{\mu}\mathrm{e}^{\mathrm{i}Ht}) \\ &= Tr(\rho^{1/4}\vec{\mu}^{\dagger}\rho^{1/4}\mathrm{e}^{-\mathrm{i}Ht}\rho^{1/4}\vec{\mu}\rho^{1/4}\mathrm{e}^{\mathrm{i}Ht}),\end{aligned} \tag{5}$$

one is able to express $\tilde{F}(\omega)$ as

$$\tilde{F}(\omega) = -\frac{1}{\pi}\,\mathrm{Im}\,Tr\left\{\rho^{1/4}\vec{\mu}^{\dagger}\rho^{1/4}\,\frac{1}{\omega-\mathscr{L}}\,\rho^{1/4}\vec{\mu}\rho^{1/4}\right\}. \tag{6}$$

In the above expression, the Liouville operator $\mathscr{L}$ associated with the total Hamiltonian H is defined as

$$\mathscr{L}A \equiv HA - AH, \tag{7}$$

where A is an arbitrary operator in Hilbert space.

In the present study, we only consider low-pressure cases in which both the water vapor density and the nitrogen buffer density are low. Based on the binary collision approximation, one can further focus on a single H_2O–N_2 pair and neglect its correlation with others. As a result, the absorption coefficient $\alpha(\omega)$ of the whole gas sample can be expressed as

$$\alpha(\omega) = n_{\mathrm{pair}}\,\frac{8\pi^2}{3\hbar c}\,\omega \sinh(\beta\hbar\omega/2)\tilde{F}(\omega), \tag{8}$$

where n_{pair} is the number density of pairs and it is proportional to the product of the pressures of H_2O and N_2; $\tilde{F}(\omega)$ is the spectral density of the pair whose expressions are the same as Eq. (6), except all the quantities belong to the pair only. For simplicity, we do not introduce new symbols for the two-molecule system. The Liouville operator $\mathscr{L}$ can be expressed as the sum of its components

$$\mathscr{L} = \mathscr{L}_a + \mathscr{L}_b + \mathscr{L}_1, \tag{9}$$

corresponding to the unperturbed H_2O molecule, the unperturbed N_2, and the anisotropic interaction between H_2O and N_2.

In the present study, the frequencies of interest are only a few cm^{-1} which are much smaller than the strong resonance line frequencies. As shown later, during collision processes, the anisotropic interaction can cause millimeter wave continuum absorptions when H_2O and N_2 have separations beyond 3.5 Å. It is well known that at this range, the whole interaction is rather weak and the anisotropic part is even weaker. Therefore, one can conclude that not only $V_{\mathrm{iso}}(r) < H_a$, but also $V_{\mathrm{ani}}(r) < H_a$. We note that based on the latter, we can draw a further conclusion that $\mathscr{L}_1 < \mathscr{L}_a$, which will be used in our later discussions. Then, we can introduce the approximation $\rho \simeq \rho_a\rho_b\rho_{\mathrm{iso}}$ in Eq. (6) and, in addition, we can exclude the component $\mathscr{L}_b$ from $\mathscr{L}$ because H_b commutes with

$(\rho_a\rho_b\rho_{\rm iso})^{1/4}\vec{\mu}(\rho_a\rho_b\rho_{\rm iso})^{1/4}$. By dividing all degrees of freedom of the two interacting molecules into internal and translational degrees, we rewrite the expression for $\tilde{F}(\omega)$ as

$$\tilde{F}(\omega) = -\frac{1}{\pi}\,\mathrm{Im}\,Tr_r\left\{\rho_{\rm iso}Tr_{ab}[\rho_a^{1/4}\vec{\mu}^{\dagger}\rho_a^{1/4}\sqrt{\rho_b}\,\frac{1}{\omega-\mathscr{L}}\sqrt{\rho_b}\rho_a^{1/4}\vec{\mu}\rho_a^{1/4}]\right\}. \tag{10}$$

In the above expression, the trace operator Tr_{ab} is over the internal degrees and the trace operator Tr_r is over the translational degrees. It turns out that to carry out Tr_{ab} is much more difficulty than Tr_r. Therefore, we focus our attention on Tr_{ab} first and apply the Lanczos algorithm to solve the problem.

2.2. Lanczos algorithm

We do not describe this method in detail here, rather the reader is referred to the review by Moro and Freed and references therein [19]. In line space, the Liouville operator $\mathscr{L}$ and therefore the resolvent operator $(\omega-\mathscr{L})^{-1}$ are matrix operators; ordinary (in Hilbert space) operators for instance, $(\rho_a\rho_b)^{1/4}\vec{\mu}(\rho_a\rho_b)^{1/4}$ are vectors. One begins by defining a starting vector (in line space)

$$|1\rangle = |v\rangle/\sqrt{\langle v|v\rangle}, \tag{11}$$

where $|v\rangle \equiv |(\rho_a\rho_b)^{1/4}\vec{\mu}(\rho_a\rho_b)^{1/4}\rangle$ and from this, one generates a complete set of basis vectors $(|1\rangle,|2\rangle,\ldots,|n\rangle,\ldots)$ according to

$$\begin{aligned}
\beta_2|2\rangle &= (1-P_1)\mathscr{L}|1\rangle,\\
\beta_3|3\rangle &= (1-P_2)\mathscr{L}|2\rangle,\\
&\vdots\\
\beta_n|n\rangle &= (1-P_{n-1})\mathscr{L}|n-1\rangle.
\end{aligned} \tag{12}$$

In these expressions, P_n are the projection operators

$$P_n = \sum_{i=1}^{n}|i\rangle\langle i| \tag{13}$$

and the quantities β_n are determined from the normalization requirement ($\langle n|n\rangle = 1$); these are given by

$$\beta_n = \langle n|\mathscr{L}|n-1\rangle \quad for\ n>1. \tag{14}$$

The matrix representation of $\mathscr{L}$ in line space given in the complete basis $(|1\rangle,|2\rangle,\ldots)$ has the symmetric tridiagonal form whose off-diagonal elements are β_n $(n=2,3,\ldots)$ and whose diagonal elements, α_n $(n=1,2,\ldots)$, are given by

$$\alpha_n = \langle n|\mathscr{L}|n\rangle. \tag{15}$$

Then, one can write the inner trace of $\tilde{F}(\omega)$ in terms of a continued fraction

$$Tr_{ab}\left[\rho_a^{1/4}\vec{\mu}^{\dagger}\rho_a^{1/4}\sqrt{\rho_b}\,\frac{1}{\omega-\mathscr{L}}\,\sqrt{\rho_b}\rho_a^{1/4}\vec{\mu}\rho_a^{1/4}\right]=\left\langle v\left|\frac{1}{\omega-\mathscr{L}}\right|v\right\rangle$$

$$=\langle v|v\rangle\frac{1}{\omega-\alpha_1-\dfrac{\beta_2^2}{\omega-\alpha_2-\dfrac{\beta_3^2}{\omega-\alpha_3-\cdots}}}. \tag{16}$$

It is worth mentioning that all quantities $\langle v|v\rangle$, α_n, and β_n appearing in the continued fraction expression are matrix elements. However, except for $\langle v|v\rangle$, their values can vary because $\mathscr{L}_1$ depends on the separation r between the two molecules; thus α_n and β_n depend on r also. As shown later, the translational motion of two molecules can be treated classically so that one can consider r as a parameter here. All these α_n and β_n^2 can be given in terms of matrix elements of $\mathscr{L}$ and its powers between the starting vector $|1\rangle$. The expressions for those appearing explicitly in Eq. (16) have been given in our recent paper [18] and will not presented here.

The continued fraction expression for $\tilde{F}(\omega)$ is the starting formula to carry out numerical calculations. In practice, one has to introduce a cut-off in Eq. (16) to limit fractions included and to make sure results obtained accordingly are converged. A simple convergence criterion is the requirement

$$\beta_n^2 \ll \alpha_{n-1}\alpha_n \quad \text{for } n>1. \tag{17}$$

When the lowest order cut-off is chosen, the continued fraction is simply $(\omega-\alpha_1)^{-1}$ and there is only one matrix element $\langle 1|\mathscr{L}|1\rangle$ required. For the next cut-off, one needs to calculate α_1, β_2^2, and α_2. This implies that one needs to know $\langle 1|\mathscr{L}^2|1\rangle$ and $\langle 1|\mathscr{L}^3|1\rangle$ as well. If one goes one step further, β_3^2 and α_3 are needed and two additional matrix elements $\langle 1|\mathscr{L}^4|1\rangle$ and $\langle 1|\mathscr{L}^5|1\rangle$ are required. Because $\mathscr{L}_a$ is the dominant part of $\mathscr{L}$, we can calculate the matrix elements $\langle 1|\mathscr{L}_a^i|1\rangle$ with $i=1,2,\ldots$ first and treat contributions from $\mathscr{L}_1$ as corrections. We note that the former are independent of the parameter r while the latter are functions of r.

2.3. Two starting vectors

By neglecting contributions from $\mathscr{L}_1$, we can easily evaluate α_1, β_2^2, α_2, β_3^2, and α_3 which are just 5 numbers. However, it turns out that the magnitudes of α_1, α_2, and α_3 are zero and this causes a failure of the convergence criterion Eq. (17). This is due to the cancellation between positive resonance lines of H_2O and negative resonance ones. Therefore, in order to guarantee convergence, one can divide $|v\rangle$ into two parts: $|v\rangle_+$ associated with the positive resonance lines, and $|v\rangle_-$ with the negative resonance ones. The physical meaning of this division is to separate an average over the whole band of H_2O into two averages, one over the positive resonance lines and the other over the negative resonance ones.

Using $|v\rangle_+$ and $|v\rangle_-$, the inner trace of $\tilde{F}(\omega)$ can be expressed as a sum over two terms

$$Tr_{ab}\left[\rho_a^{1/4}\vec{\mu}^{\dagger}\rho_a^{1/4}\sqrt{\rho_b}\,\frac{1}{\omega-\mathscr{L}}\,\sqrt{\rho_b}\rho_a^{1/4}\vec{\mu}\rho_a^{1/4}\right]$$

$$={}_+\left\langle v\left|\frac{1}{\omega-\mathscr{L}}\right|v\right\rangle_+ + {}_-\left\langle v\left|\frac{1}{\omega-\mathscr{L}}\right|v\right\rangle_-. \tag{18}$$

By following the same procedure as described above, we can rewrite each term as a continued fraction as in Eq. (16). Accordingly, there are two sets of α_n and β_n^2 to be evaluated. However, these two sets are not independent. In fact, the β_n^2 are identical and the α_n have the same magnitudes, but different signs. Therefore, we need only to carry out calculations of α_n and β_n^2 associated with one set, say, with $|v\rangle_+$.

The explicit expression for the line space vector $|v\rangle_+$ is given by

$$|v\rangle_+ = \sum_{j\tau m}\sum_{j'\tau' m'}\sum_{ln}\left\{\sqrt{g_l}\mathrm{e}^{-\beta E(l)/2}(g_\tau g_{\tau'})^{1/4}\mathrm{e}^{-\beta[E(j,\tau)+E(j',\tau')]/4} \times \langle j\tau m|\vec{\mu}|j'\tau' m'\rangle/\sqrt{Q_a Q_b}\right\} \times |j\tau m ln\rangle\langle j'\tau' m' ln|, \tag{19}$$

where $|j\tau m ln\rangle$ is a simple notation for $|j\tau m\rangle \otimes |ln\rangle$, g_τ and g_l are the nuclear spin degeneracy factors for H_2O and N_2, Q_a and Q_b are the partition functions of H_2O and N_2, respectively, and the summation over j' and τ' is limited to a range with $E(j',\tau') < E(j,\tau)$. We introduce a normalization constant M_+ defined by

$$M_+ = \sum_{j\tau}\sum_{\{j'\tau'\}_+}(2J+1)\sqrt{g_\tau g_{\tau'}}\mathrm{e}^{-\beta[E(j,\tau)+E(j',\tau')]/2}|\mu_{j\tau;j'\tau'}|^2/Q_a, \tag{20}$$

where the summation indicated by the symbol $\{j'\tau'\}_+$ is limited to a range with $E(j',\tau') < E(j,\tau)$. In the above expression, $\mu_{j\tau;j'\tau'}$ are associated with the reduced dipole matrix elements, but exclude the magnitude μ of the dipole operator of H_2O; their expression has been given in Ref. [18]. It is obvious that ${}_+\langle v|v\rangle_+ = \mu^2 M_+$.

2.4. Matrix elements of ${}_+\langle 1|\mathscr{L}^i|1\rangle_+$

Based on a binomial expansion of $(\mathscr{L}_a + \mathscr{L}_1)^i$, there are 2^i terms of ${}_+\langle 1|\mathscr{L}^i|1\rangle_+$ which can be catalogued into $i+1$ groups according to the powers of $\mathscr{L}_1$. The group without $\mathscr{L}_1$ present contains only one term ${}_+\langle 1|\mathscr{L}_a^i|1\rangle_+$ and can be expressed as

$${}_+\langle 1|\mathscr{L}_a^i|1\rangle_+ = \frac{1}{M_+}\sum_{j\tau}\sum_{\{j'\tau'\}_+}(2J+1)\sqrt{g_\tau g_{\tau'}}\mathrm{e}^{-\beta[E(j,\tau)+E(j',\tau')]/2} \times|\mu_{j\tau;j'\tau'}|^2\{E(j,\tau)-E(j',\tau')\}^i/Q_a. \tag{21}$$

By including all states of H_2O up to $J_{\max}=26$, we can easily calculate ${}_+\langle 1|\mathscr{L}_a^i|1\rangle_+$ for $i=1,2,3,4$, and 5 from Eq. (21); for $T = 296$ K, we obtain the corresponding values: 104.850 cm^{-1}, 15351.0 cm^{-2}, 2.86506×10^6 cm^{-3}, 6.42481×10^8 cm^{-4}, and 1.66650×10^{11} cm^{-5}, respectively.

If one ignores contributions from other groups containing $\mathscr{L}_1$ and its powers, we obtain $\alpha_1 =$ 104.850 cm^{-1}, $\beta_2^2 = 4357.56$ cm^{-2}, $\alpha_2 = 183.275$ cm^{-1}, $\beta_3^2 = 10345.51$ cm^{-2}, and $\alpha_3 = 246.611$ cm^{-1}. From these values, it is easy to check that the convergence criterion is satisfied because $\beta_2^2/(\alpha_1\alpha_2) =$ 0.227 and $\beta_3^2/(\alpha_2\alpha_3) = 0.229$. Based on these values, explicit expressions for $\tilde{F}(\omega)$ in terms of the two continued fraction are known. Then, one can easily find the poles of the fractions on the ω axis. For the lowest-order cut-off, there are two poles: $\omega = 104.850$ cm^{-1} and $\omega = -104.850$ cm^{-1},

one from each of the continued fractions, respectively. For the next order, there are four poles: $\omega =$ 67.282 cm^{-1}, 220.843 cm^{-1} and $\omega = -67.282$ cm^{-1}, -220.843 cm^{-1} associated with $|1\rangle_+$ and $|1\rangle_-$, respectively. Similarly, for the next higher-order shown explicitly in Eq. (16), there are six poles: $\omega = 50.4437$, 155.566, 328.727 cm^{-1} and $\omega = -50.4437$, -155.566, -328.727 cm^{-1}, respectively. As shown by these numbers, the poles of these two continued fractions are symmetrically located about the origin of the ω axis. Because there is no pole within the millimeter spectral region, it seems that without considering the interaction between H_2O and N_2, there are no local line absorptions in this region at all. Clearly, the above statement is not correct because there are a few relatively weak lines there. But, given the fact that most of the lines of the pure rotational band are located beyond the millimeter spectral region, and that results from the Lanczos algorithm represent averaged effects mainly over these lines, our finding is consistent. This implies that it is the anisotropic interaction that plays the crucial role in causing the millimeter wave absorption.

Our next effort is to calculate contributions from other groups. As shown later, due to anti-symmetry of their integrand, the matrix elements of the terms linear in $\mathscr{L}_1$ are zero. Thus, we need to consider groups whose terms contain $\mathscr{L}_1^2$ and higher powers. At this stage, if one uses the usual method to evaluate the corresponding matrix elements, the calculations becomes intractable. We can circumvent this by introducing the coordinate representation. We do not discuss the advantages of coordinate representation here, but simply claim that no matter how complicated $\mathscr{L}_1$ is or how many powers of $\mathscr{L}_1$ appear in these terms, they are just multidimensional integrations with ordinary functions as integrands that can be successfully evaluated using the Monte Carlo method [15,16].

As an example, we show how to calculate the matrix element ${}_+\langle 1|\mathscr{L}^2|1\rangle_+$ here. This matrix element contains 4 terms which can be cataloged into 3 groups

$$ {}_+\langle 1|\mathscr{L}^2|1\rangle_+ = {}_+\langle 1|\mathscr{L}_a^2|1\rangle_+ + {}_+\langle 1|\mathscr{L}_1\mathscr{L}_a|1\rangle_+ + {}_+\langle 1|\mathscr{L}_a\mathscr{L}_1|1\rangle_+ + {}_+\langle 1|\mathscr{L}_1^2|1\rangle_+. \tag{22}$$

The first term does not contain $\mathscr{L}_1$ and its value is already known. The second and third terms are linear in $\mathscr{L}_1$. We adopt the notation that $\Omega_{a\zeta}$ is used to represent the orientation of H_2O with three Euler angles α_ζ, β_ζ, and γ_ζ and $\Omega_{b\zeta}$ for N_2 with the two angles θ_ζ and φ_ζ. Then, we can express the basis function $|\zeta\rangle$ in the coordinate representation as

$$ |\zeta\rangle = |\delta(\Omega_a - \Omega_{a\zeta})\delta(\Omega_b - \Omega_{b\zeta})\rangle. \tag{23}$$

We note that these basis functions are eigenfunctions of V_{ani},

$$ V_{\mathrm{ani}}(r, \Omega_a, \Omega_b)|\zeta\rangle = V_{\mathrm{ani}}(r, \Omega_{a\zeta}, \Omega_{b\zeta})|\zeta\rangle, \tag{24}$$

where $V_{\mathrm{ani}}(r, \Omega_{a\zeta}, \Omega_{b\zeta})$ are the eigenvalues; i.e., they are simply values of V_{ani} at positions of the pair specified by r, $\Omega_{a\zeta}$, and $\Omega_{b\zeta}$. For simplicity, we will denote $V_{\mathrm{ani}}(r, \Omega_{a\zeta}, \Omega_{b\zeta})$ by $V_{\mathrm{ani}}(\zeta)$. In terms of this basis set, one is able to rewrite the second term ${}_+\langle 1|\mathscr{L}_1\mathscr{L}_a|1\rangle_+$ as

$$ {}_+\langle 1|\mathscr{L}_1\mathscr{L}_a|1\rangle_+ = \frac{1}{M_+}\iint \mathrm{d}\Omega_\zeta \mathrm{d}\Omega_\eta [V_{\mathrm{ani}}(\zeta) - V_{\mathrm{ani}}(\eta)] \times \langle \eta|\rho_a^{1/4}\vec{\mu}_+^{\dagger}\rho_a^{1/4}\sqrt{\rho_b}|\zeta\rangle\langle\zeta|\sqrt{\rho_b}\mathscr{L}_a\rho_a^{1/4}\vec{\mu}_+\rho_a^{1/4}|\eta\rangle, \tag{25}$$

where $\mathrm{d}\Omega_\zeta$ denotes the volume element and the subscript $+$ of μ_+ implies that its components lie in a subspace constructed from the positive resonance lines only. Because the integrand in Eq. (25) is

anti-symmetric with respect to ζ and η, the value of this term is zero. Similarly, we can conclude that the third term is zero too.

The last term is given by

$$ {}_+\langle 1|\mathscr{L}_1^2|1\rangle_+ = \frac{1}{M_+}\iint \mathrm{d}\Omega_\zeta\,\mathrm{d}\Omega_\eta[V_{\mathrm{ani}}(\zeta)-V_{\mathrm{ani}}(\eta)]^2 \times\langle\eta|\rho_a^{1/4}\vec{\mu}_+^{\dagger}\rho_a^{1/4}\sqrt{\rho_b}|\zeta\rangle\langle\zeta|\sqrt{\rho_b}\rho_a^{1/4}\vec{\mu}_+\rho_a^{1/4}|\eta\rangle. \tag{26}$$

The original dimensionality of the integration in Eq. (26) is 10. However, due to the rotational symmetry of the system about the z-axis in the space-fixed frame, one can always reduce the dimensionality by one. Then, using the Monte Carlo method, we can carry out the multidimensional integrations in which the integrand is an ordinary function. Although using the coordinate representation and the Monte Carlo method enables us to calculate the matrix element ${}_+\langle 1|\mathscr{L}_1^2|1\rangle_+$, the calculation is still time consuming. We have developed helpful techniques including the use of distribution functions to handle the calculation. Because these techniques have been explained in detail in our recent work [14–16], we do not discuss them here. Finally, as mentioned previously, this matrix element depends on the parameter r. In practice, we select 80 values of r to cover the whole range of the interaction between H_2O and N_2 and calculate the corresponding matrix elements. Similarly, we can calculate matrix elements ${}_+\langle 1|\mathscr{L}^3|1\rangle_+$, ${}_+\langle 1|\mathscr{L}^4|1\rangle_+$, and ${}_+\langle 1|\mathscr{L}^5|1\rangle_+$. Detailed discussions about these calculations can be found in our recent paper [18].

2.5. Interaction potential

It is well known that the interaction potential, especially its anisotropic part, plays a crucial role in pressure broadening, as is the case here. This implies that in the theoretical modeling, one has to adopt a potential model that is as accurate as possible. Within the present formalism, one is free to choose any isotropic potential model $V_{\mathrm{iso}}(r)$ because $V_{\mathrm{iso}}(r)$ appears only in Tr_r (but not in Tr_{ab}), and thus only needs to be calculated once. In our recent work, we adopted a Lennard-Jones model with the two parameters $\varepsilon = 3.40$ Å and $\sigma/k = 168.0$ K.

With respect to the anisotropic potential, there is a practical limit to the choice of models because their values have to be evaluated billions times in the calculations. Thus, one has to select anisotropic models with relatively simple forms and a modest number of parameters. As shown later, it is the middle-range anisotropic part that plays the main role in determining the millimeter wave foreign continuum. Therefore, it is essential to adopt a model whose middle-range anisotropic part is as accurate as possible. Because the H_2O molecule has a large dipole moment, the middle-range anisotropic potential can be well modeled by the dipole–quadrupole interaction

$$V_{\mathrm{dq}}(r,\Omega_a,\Omega_b) = \frac{3\mu\Theta}{2r^4}\,[\cos\beta_a(3\cos^2\theta_b-1)-2\sin\beta_a\sin\theta_b\cos\theta_b\cos(\alpha_a-\varphi_b)], \tag{27}$$

where μ and Θ are values of the dipole of H_2O and the quadrupole of N_2, respectively, and $\mu = 1.8546$ D and $\Theta = 1.466$ D Å are well known. We note that in writing the above expression, one adopts the II^r representation of H_2O in which the dipole moment lies along the Z-axis of molecule-fixed frame. With Eq. (27), one can conclude that the dipole–quadrupole interaction

contains a cyclic coordinate because it is independent of the Euler angle γ_a of H_2O. Then, if the short-range potential model used also has the same symmetry, it is possible to reduce the required numerical calculations dramatically. In general, the dimensionality of the integration over angular variables for the H_2O–N_2 pair, is 9. However, because the potential is independent of γ_a, two integrations over the initial angle γ_a and final angle γ'_a can be carried out analytically. As a result, all the nine-dimensional integrations are reduced to seven-dimensional ones. In the present study, we adopt the same site–site model to represent short-range repulsive interaction that was used in our recent paper [18]. This model assumes that all force centers of H_2O are located along its Z-axis and has two parameters, V_0 and ρ_0. We choose their values $V_0/k = 5.0 \times 10^7$ K and $\rho_0 = 0.225$ Å in present calculations. As an independent check, we calculate theoretical predictions of the second virial coefficients (i.e., $B(T)$=34.81, 27.60, 21.62, and 16.60 cm^3/mol for T=298.15, 323.15, 348.15, and 373.15 K, respectively) which agree well with measurements (viz., $B(T)=40\pm6$, 28 ± 5, 20 ± 4, 15.5 ± 3 cm^3/mol).

2.6. Poles of the continued fractions

After obtaining the matrix elements, the most difficult job, i.e., performing the Tr_{ab} operation, is finished, and the results obtained are represented by two fractions associated with the positive and negative resonance lines, respectively. By considering ω as a variable in the complex plane, one can easily find the poles and residues from each of these fractions. However, because the two fractions are not independent, their poles have the same magnitudes, but with opposite signs. In addition, a pole belonging to one fraction and its mirror belonging to the other fraction have the same residue. As a result, we can express these two fractions as

$$ {}_+\left\langle v\left|\frac{1}{\omega-\mathscr{L}}\right|v\right\rangle_+ + {}_-\left\langle v\left|\frac{1}{\omega-\mathscr{L}}\right|v\right\rangle_- = \mu^2 M\sum_{i=1}^{3}\left\{\frac{R_i(r)}{\omega-z_i(r)}+\frac{R_i(r)}{\omega+z_i(r)}\right\}, \tag{28}$$

where $i=1,2$, and 3 resulting from a choice of the third-order cut-off used in the present study. In the above expression, $z_i(r)$ are the poles derived from the fraction associated with the positive resonance lines and $R_i(r)$ are corresponding residues. Because $|v\rangle_+$ and $|v\rangle_-$ have the same normalization constant (i.e., $M_+ = M_-$), we have used the symbol M to represent them in Eq. (28). At this stage, we have obtained six poles and three residues. Each of them is a function of r and is characterized by 80 points because we have selected 80 different r values in the calculations. In general, these poles can be complex numbers, but some are real. Among them, we are most interested in those whose values are real and located between 0 cm^{-1} and, say, ±15 cm^{-1}. We found that among the six poles there is one pole and its mirror partner which satisfy these criteria, and their values vary smoothly with r. We present these poles calculated for $T = 270$, 296, and 330 K in Fig. 1 to show how they are distributed on the frequency axis. As shown by the figure, the pair of poles obtained for $T = 296$ K are represented by two smooth curves which mirror each other, cross at around $r = 4.0$ Å, and approach asymptotic limits ±50.4437 cm^{-1}, respectively, as r goes to infinity. By comparing curves representing different temperatures, we find that the crossing distance r becomes smaller as the temperature increases. Finally, we find that the range of distances r between 3.5 and 4.5 Å is of greatest interest to us because frequency values within 0 to ±15 cm^{-1} of these curves are located there.

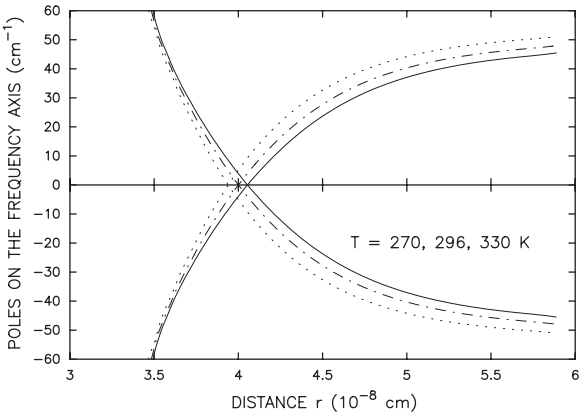

Fig. 1. The calculated poles of the continued fractions as function of r for $T=270$, 296, and 330 K. They are represented by the solid, dot-dashed, and dotted lines, respectively. For a specified temperature, there are two set of curves associated with the positive and negative resonance lines, respectively. As r increases, the positive slope curve belongs to the former and the negative one to the later.

2.7. A classical ensemble average over the translational motion

Now, we can carry out the operation Tr_r. Because the millimeter wave spectral region is far away from the strong lines of the pure-rotational band of H_2O, we introduce the quasistatic approximation in which the collisions are assumed to be of infinite duration and the translation motions can be treated classically. Then, the ensemble average of results obtained from Tr_{ab} over the translational motion becomes an integration over r from 0 to infinity with $\rho_{\rm iso}=\exp(-\beta V_{\rm iso}(r))$ as its weighting function. The latter can be easily carried out with the Cauchy's integral formula and the results are contributions to the absorption coefficients from the poles of interest. For example, let us assume that $z(r_0)$ is one pole of interest by $z(r_0)$ and its mirror are one pair of poles of interest. We can easily calculate the value of $\tilde{F}(\omega_0)$ with $\omega_0=z(r_0)$ and obtain the corresponding contribution to the absorption coefficient at this frequency

$$\alpha(\omega_0)=n_{\rm pair}\,\frac{32\pi^3}{3\hbar c}\,\omega_0\sinh(\beta\hbar\omega_0/2)\mu^2 M\,\frac{R(r_0)}{|z'(r_0)|}\,r_0^2 e^{-\beta V_{\rm iso}(r_0)}, \tag{29}$$

where $z'(r)\equiv {\rm d}z(r)/{\rm d}r$. As shown by Eq. (29), the calculation of $\alpha(\omega_0)$ is straightforward because all quantities appearing on the right-hand side of the equation are known. By combining contributions from all poles of interest, we know values of the absorption coefficients at many frequency points. Because the millimeter wave continuum absorption is a smooth function of frequency, its value at any ω can easily be found.

2.8. Numerical results and a simple parameterization for $\alpha(f,T)$

We calculate absorption coefficients of H_2O–N_2 for frequencies f below 450 GHz for a dozen temperatures ranging from 220 to 330 K. We plot the 12 results obtained for $T=220,230,\ldots,330$ K in Fig. 2. In order to compare our theoretical values with those predicted from MPM89 and MPM93,

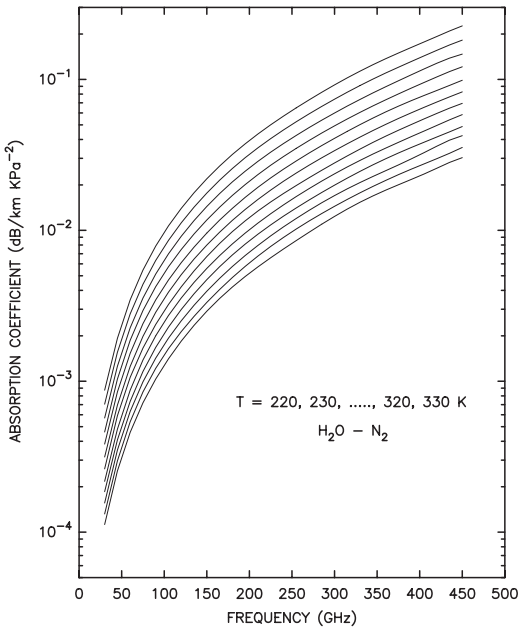

Fig. 2. The calculated H_2O–N_2 millimeter wave continuum (in units of dB/km kPa^{-2}) for $T = 220, 230, \ldots, 330$ K; these are represented by 12 lines from the top to the bottom, respectively. The results are well fitted by a simple formula: $\alpha(f,T) = AP_{H_2O}P_{N_2}f^B(300/T)^C$ with $A = 1.5915 \times 10^{-7}$, $B = 2.059$, and $C = 4.982$.

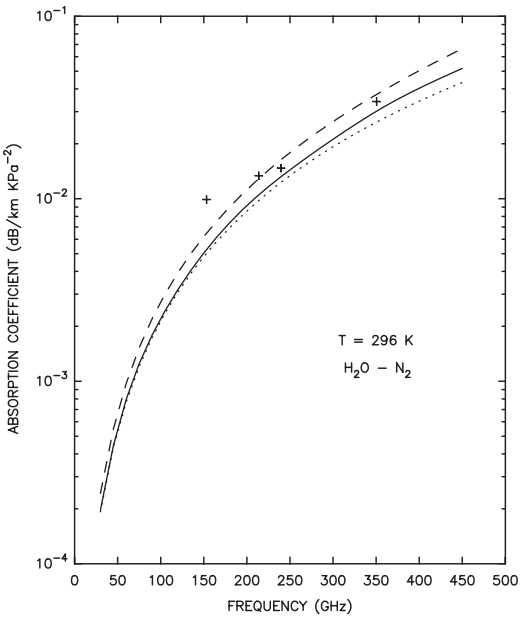

Fig. 3. The calculated $H_2O - N_2$ continuum for $T = 296$ K are represented by the solid line. The corresponding values derived from the MPM89 and MPM93 models are represented by the dotted and dashed lines, respectively. The values deduced from the Bauer et al. measurements at 153.000, 213.525, 239.370, and 350.300 GHz are represented by a symbol $+$.

we plot the results obtained for $T = 296$, 330, and 270 K in Figs. 3–5, respectively. In Figs. 3 and 4, we also plot values obtained by subtracting the local Van Vleck–Weisskopf line contributions up to 1000 GHz from the Bauer et al. measurements of $H_2O - N_2$ at 153.000, 213.525, 239.370, and 350.300 GHz, respectively. As shown in these figures, the theoretical predictions are smooth functions of the frequency and they increase almost quadratically as the frequency increases. In comparison with MPM89 and MPM93, our values lie between them. In addition, except for $f = 153.000$ GHz, our values agree well with those from the Bauer et al. measurements. Finally, in order to show the temperature dependence more clearly for the four specified frequencies $f = 153.000$, 213.525, 239.370, and 350.300 GHz, respectively, we calculate $\alpha(f,T)$ for $T = 260, 270, \ldots, 370$ K and plot $\alpha(f,T)/f^2$ in Fig. 6. As shown in the figure, they are four straight lines, the first three are almost identical and the forth is parallel with a little separation. This implies that the temperature dependence of $\alpha(f,T)$ can be well characterized by T^N where the index N is a constant. On the other hand, the frequency dependence is not exactly quadratic, but very close. We also plot the corresponding values obtained from the MPM89 and MPM93 models, and those deduced from the measurements of Bauer et al. in the same figure. Because the MPM89 model is proportional to f^2T^{-3}, it is represented by one straight line only. Meanwhile, each of the MPM93 model and Bauer et al. data is represented by four lines. As shown in the figure, our results, those of Bauer et al., and the MPM93 model exhibit

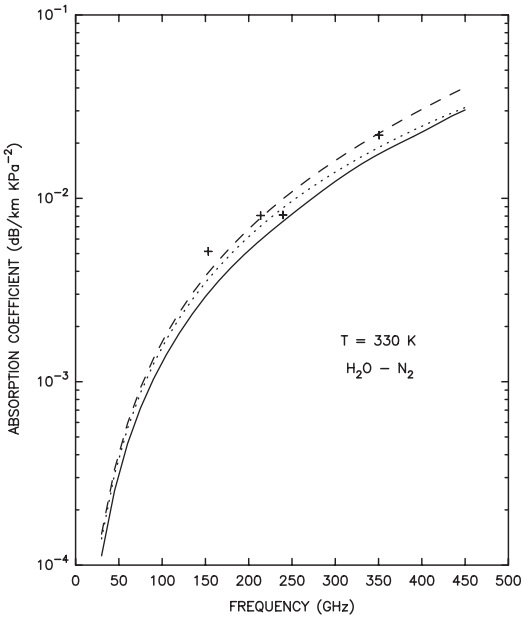

Fig. 4. The same as Fig. 3, except for $T = 330$ K.

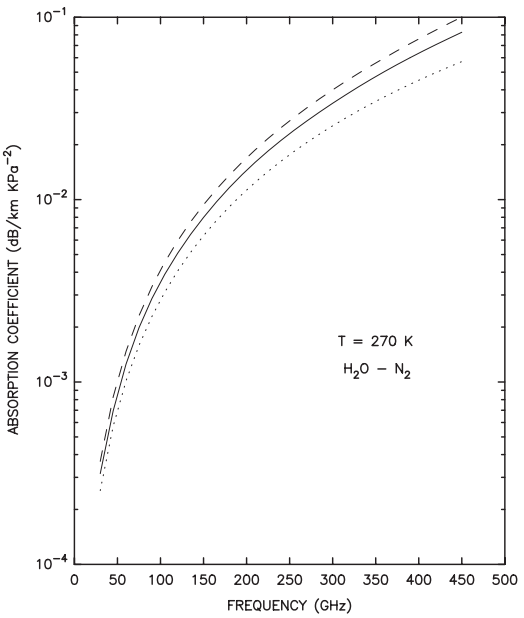

Fig. 5. The same as Fig. 3, except for $T = 270$ K and no experimental data.

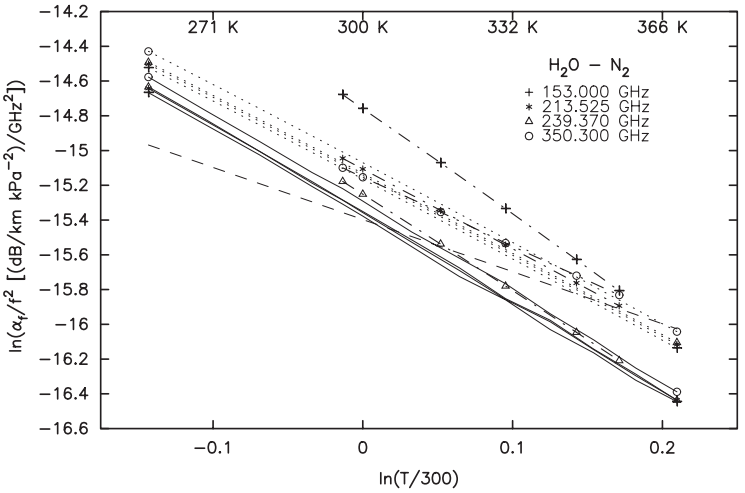

Fig. 6. A log–log plot of the calculated $H_2O - N_2$ millimeter wave continuum divided by the square of f at 153.000, 213.525, 239.370, and 350.300 GHz, respectively, as a function of the temperature. The theoretical values are represented by the solid lines with different symbols marked at their ends. Those from the MPM93 model are represented by the four dotted lines with similar end marks. Because the continuum of the MPM89 model is proportional to f^2, their values are presented by one straight dashed line. The Bauer et al. values are plotted with $+, *, \triangle$ and $\circ$, respectively; for clarity, the same symbol is linked by the dot-dashed line.

a very similar negative temperature dependence, much stronger than the MPM89 model. By fitting our results calculated for a dozen different temperatures ranging from 220 to 330 K, an analytical parameterization for the continuum (in dB/km), applicable for frequencies up to 450 GHz, can be expressed as

$$\alpha(f,T) = 1.5915 \times 10^{-7} P_{H_2O} P_{N_2} (300/T)^{4.982} f^{2.059}, \tag{30}$$

where the pressures P_{H_2O} and P_{N_2} are given in kPa. This parameterization differs slightly from our previous result [18] because different parameters V_0, ρ_0, ε, and σ have been used in the calculations. In the above expression, as expected, the frequency dependence of $\alpha(f,T)$ is very close to, but not exactly quadratic. Meanwhile, the temperature index obtained is a constant -4.982 which differs significantly from -3 of the MPM89 model. Finally, we note that the above formula represents the calculated continuum only, and contributions from individual lines must be added to obtain the absorption coefficient [20].

3. Discussion and conclusions

From the work presented above, we can draw several conclusions. First, the Lanczos algorithm, when carried out in the coordinate representation and using the Monte Carlo method to compute accurately the multidimensional integrations, is a powerful tool for calculating the water vapor millimeter wave foreign continuum. This absorption is due to the anisotropic interaction potential; more specifically, to the range of separations between 3.5 and 4.5 Å, where it can be well represented by the dipole–quadrupole term. In general, the theoretical results are in good agreement with the experimental results of Bauer et al. (except for the results at 153 GHz), especially considering the difficulty of the measurements and the data reduction needed to extract the weak foreign continuum. When compared to the empirical results of Liebe, our results lie between the MPM89 and MPM93 models, but the temperature dependence is closer to the latter model. Clearly, the T^{-3} dependence assumed in the MPM89 model, which ignores the T-dependence of the spectral density that contains information about the collisional process, is not a good approximation, whereas the (approximate) quadratic dependence on the frequency is reasonably good.

Second, while there are several refinements that can be made to the present theoretical results, what is needed most are more accurate experimental and/or field data. In particular, it would be useful to obtain laboratory data at lower temperatures and at higher frequencies. At the same time, intercomparisons of field data and the sensitivity of retrieved quantities to the continuum parametrizations (both self and foreign) could shed light on where the empirical or theoretical models could be improved.

Finally, we note that at the higher frequencies, the "dry continuum" due to the collision-induced absorption in N_2–N_2, N_2–O_2, and $O_2 - O_2$ pairs has to be taken into account. While the N_2–N_2 absorption is contained in the various empirical models, we have recently shown [21] that the absorption of $N_2 - O_2$ increases this by approximately 35%, and should be included.

Acknowledgements

This research was supported by the Biological and Environmental Research Program (BER), US Department of Energy, Interagency Agreement No. DE-AI02-93ER61744 and by NASA through

grant NAG5-8269. The authors would like to thank the National Energy Research Supercomputer (Livermore, CA) for computer time and facilities provided. Also, we would like to thank Dr. A. Bauer for useful discussions.

References

[1] Read WG, Waters JW, Wu DL, Stone EM, Shippony Z, Smedley AC, Smallcomb CC, Oltmans S, Kley D, Smit HGJ, Mergenthaler JL, Karki MK. UARS Microwave limb sounder upper tropospheric humidity measurements: method and validation. J Geophys Res 2001;106:32207–58.
[2] Rosenkranz PW. Water vapor microwave continuum absorption: a comparison of measurements and models. Radio Sci 1998;33:919–28 (Correction Radio Sci 1999;34:1025).
[3] Liebe HJ. The atmospheric water vapor continuum below 300 GHz. Int J Infrared Millimeter Waves 1984;5: 207–27.
[4] Liebe HJ, Layton DH. Millimeter-wave properties of the atmosphere: laboratory studies and propagation modeling. NTIA Report 87-224, Natl Telecommun and Inf Admin, Boulder, CO, 1987.
[5] Bauer A, Godon M. Temperature dependence of water-vapor absorption in linewings at 190 GHz. JQSRT 1991;46:211–20.
[6] Godon M, Carlier J, Bauer A. Laboratory studies of water vapor absorption in the atmospheric window at 213 GHz. JQSRT 1992;47:275–85.
[7] Bauer A, Godon M, Carlier J, Ma Q, Tipping RH. Absorption by H_2O and H_2O–N_2 mixtures at 153 GHz. JQSRT 1993;50:463–75.
[8] Bauer A, Godon M, Carlier J, Ma Q. Water-vapor absorption in the atmospheric window at 239 GHz. JQSRT 1995;53:411–23.
[9] Kuhn T, Bauer A, Godon M, Bühler S, Künzi K. Water vapor continuum: absorption measurements at 350 GHz and model calculations. JQSRT 2002;74:545–62.
[10] Liebe HJ. MPM—an atmospheric millimeter-wave propagation model. Int J Infrared Millimeter Waves 1989;10: 631–50.
[11] Liebe HJ, Hufford GA, Cotton MG. Propagation modeling of moist air and suspended water/ice particles at frequencies below 1000 GHz. AGARD Conference Proceedings 1993;542:3–10.
[12] Clough SA, Kneizys FX, Davies RW. Line shape and the water vapor continuum. Atmos Res 1989;23:229–41.
[13] Pardo JR, Serabyn E, Cernicharo J. Submillimeter atmospheric transmission measurements on Mauna Kea during extremely dry El Niño conditions: implications for broadband opacity contributions. JQSRT 2001;68:419–33.
[14] Ma Q, Tipping RH. The averaged density matrix in the coordinate representation: application to the calculation of the far-wing line shapes for H_2O. J Chem Phys 1999;111:5909–21.
[15] Ma Q, Tipping RH. The density matrix of H_2O–N_2 in the coordinate representation: a Monte Carlo calculation of the far-wing line shape. J Chem Phys 2000;112:574–84.
[16] Ma Q, Tipping RH. The frequency detuning correction and the asymmetry of line shapes: the far wings of H_2O–H_2O. J Chem Phys 2002;116:4102–15.
[17] Ma Q, Tipping RH. Water vapor continuum in the millimeter spectral region. J Chem Phys 1990;93:6127–39.
[18] Ma Q, Tipping RH. Water vapor millimeter wave foreign continuum: a Lanczos calculation in the coordinate representation. J Chem Phys 2002;117:10581–96.
[19] Moro G, Freed JH. The Lanczos algorithm in molecular dynamics: calculation of spectral densities. In: Cullum J, Willough RA, editors. Large scale eigenvalue problems. Amsterdam: Elsevier Science Publishers B.V., Amsterdam: North Holland, 1986. p. 143–60.
[20] Rothman LS, Rinsland CP, Goldman A, Massie ST, Edwards DP, Flaud J-M, Perrin A, Camy-Peyret C, Dana V, Mandin JY, Schroeder J, McCann A, Gamache RR, Wattson RB, Yoshino K, Chance KV, Jucks JW, Brown LR, Nemtchinov V, Varanasi P. The HITRAN molecular spectroscopic database and HAWKS (HITRAN Atmospheric Workstation): 1996 edition. JQSRT 1998;60:665–710.
[21] Boissoles J, Boulet C, Tipping RH, Brown A, Ma Q. Theoretical calculation of the translation-rotation collision-induced absorption in N_2–N_2, O_2–O_2, and N_2–O_2 pairs. JQSRT, doi:10.1016/S0022-4073(03)00174-2.